Biogeosciences Discuss., 6, 291–340, 2009
www.biogeosciences-discuss.net/6/291/2009/

Biogeosciences Discussions

Biogeosciences Discussions is the access reviewed discussion forum of *Biogeosciences*

Direct contribution of phytoplankton-sized particles to optical backscattering in the open ocean

G. Dall'Olmo[1], T. K. Westberry[1], M. J. Behrenfeld[1], E. Boss[2], and W. H. Slade[2]

[1]Department of Botany and Plant Pathology, 2082 Cordley Hall, Oregon State University, Corvallis, OR 97331, USA
[2]MISC Lab, University of Maine, 458 Aubert Hall, Orono, ME 04469, USA

Received: 29 October 2008 – Accepted: 12 November 2008 – Published: 8 January 2009

Correspondence to: G. Dall'Olmo (giorgiod@science.oregonstate.edu)

Published by Copernicus Publications on behalf of the European Geosciences Union.

Abstract

Light scattering properties of oceanic particles have been suggested as an alternative index of phytoplankton biomass than chlorophyll-*a* concentration (chl-*a*), with the benefit of being less sensitive to physiological forcings (e.g., light and nutrients) that alter the intracellular pigment concentrations. The drawback of particulate scattering is that it is not unique to phytoplankton. Nevertheless, field studies have demonstrated that, to first order, the particulate beam-attenuation coefficient (c_p) can track phytoplankton abundance. The relationship between c_p and the particulate backscattering coefficient (b_{bp}), a property retrievable from space, has not been fully evaluated, largely due to a lack of open-ocean field observations. Here, we present extensive data on inherent optical properties from the Equatorial Pacific surface waters and demonstrate a remarkable coherence in b_{bp} and c_p. Coincident measurements of particle size distributions (PSDs) and optical properties of size-fractionated samples indicate that this covariance is due to both the conserved nature of the PSD and a greater contribution of phytoplankton-sized particles to b_{bp} than theoretically predicted. These findings suggest that satellite-derived b_{bp} could provide similar information on phytoplankton biomass in the open ocean as c_p.

1 Introduction

Inherent optical properties (IOPs) have been recognized as important tools to study many ecophysiological and biogeochemical oceanic processes at sub-meter spatial scales and at high temporal resolution. For example, IOP data have permitted deriving phytoplankton cell sizes (Ciotti et al., 2002) and provided growth-rate estimates of particulate organic matter (Siegel et al., 1989; Claustre et al., 1999). Understanding how different types of oceanic particles affect the bulk inherent optical properties is fundamental for inferring particle dynamics and ecosystem rates from in-situ and satellite-inverted IOPs.

BGD

6, 291–340, 2009

The contribution of oceanic microorganisms to IOPs such as the particle beam-attenuation and scattering coefficients (c_p and b_p, respectively) have been investigated rather extensively by means of flow cytometry (Durand and Olson, 1996; Chung et al., 1996, 1998; Claustre et al., 1999; Green et al., 2003; Oubelkheir et al., 2005; Grob et al., 2007). Typically, the concentrations, sizes, and refractive indices of specific groups of microorganisms were estimated and then their contribution to c_p calculated.

In some of these investigations, the observed microorganisms (autototrophs and heterotrophs) accounted for a rather constant fraction of c_p, while the remaining fraction of c_p was attributed to an unmeasured particle pool referred to as "detritus" (Chung et al., 1996, 1998; Claustre et al., 1999; Oubelkheir et al., 2005). A corollary of these findings is that it should be possible to estimate the attenuation by microorganisms from bulk c_p measurements (Chung et al., 1998). By further considering that the abundances of autotrophic and heterotrophic microbes covary in the open-ocean over large scales (Cole et al., 1988; Gasol and Duarte, 2000), we can then conclude that, to first order, bulk c_p should be proportional to phytoplankton c_p.

Other studies estimated that phytoplankton accounted for up to 50–60% of c_p (Durand and Olson, 1996; Chung et al., 1996; Green et al., 2003). In addition, Durand and Olson (1996) showed that most of the diel variations in bulk c_p could be attributed to variations in phytoplankton c_p. Thus, in these investigations a first order correlation emerged directly between bulk c_p and phytoplankton c_p.

Unfortunately, a validation of the above estimates was only presented by Green et al. (2003) who favorably compared the reconstructed total particulate scattering signals to independently measured bulk b_p. Indeed, most of the aforementioned investigations adopted different hypotheses to which the calculated scattering cross-sections are strongly dependent: for example, some studies employed forward scattering measurements to obtain particle sizes (Durand and Olson, 1996; Chung et al., 1998; Green et al., 2003; Grob et al., 2007), while others assumed fixed sizes for a given particle type (Chung et al., 1996; Claustre et al., 1999; Oubelkheir et al., 2005). Thus, it is unclear if the differences in the reported contributions of microorganisms to bulk c_p were

real and due to variations in the geographic regions, or biased because of the initial hypotheses.

Regardless, we have explained why a correlation between c_p and phytoplankton abundance (the first order driver of phytoplankton c_p) is expected. Certainly this global correlation may break down at more regional scales, but it provides a way to derive phytoplankton biomass alternative to chlorophyll-*a* concentration (chl-*a*). In fact, despite its historical acceptance as an index of phytoplankton biomass, chl-*a* is also strongly influenced by physiological forcing such as light availability and nutrient stress (e.g., Geider et al., 1998). The chl-*a*:c_p ratio should thus reveal these physiological variations by removing the biomass dependence from chl-*a*.

To test this hypothesis, Behrenfeld and Boss (2003) analyzed existing time-series of data and found a correlation between chl-*a*-normalized c_p and a ^{14}C-based photoacclimation index. These investigators later assumed that c_p correlates with the particulate backscattering (b_{bp}) in the open ocean and derived relationships between satellite-based chl-*a*:b_{bp} and environmental variables that closely mimic the chl-*a*-to-carbon ratios measured in laboratory cultures of phytoplankton (Behrenfeld et al., 2005). Thus, these studies support the hypothesis that phytoplankton biomass correlates with c_p and b_{bp} in the open ocean.

This new scattering-based approach for interrogating variability in phytoplankton ecophysiology from space still has a critical knowledge gap: it is not yet clear the extent to which a direct connection exists between c_p and b_{bp} at the global scale. An exception is the recent analysis by Huot et al. (2008) that reported strong correlations in the South Pacific between both b_p or b_{bp} and chl-*a* and, by extension, between b_p and b_{bp}. Note that b_p and c_p are here used interchangeably because b_p dominates c_p in the open ocean (e.g., Loisel and Morel, 1998).

Despite this recent study, the relationship between c_p and b_{bp} is not well understood in the open ocean, mostly due to the lack of coincident c_p and b_{bp} measurements. Theoretical simulations for homogeneous spherical particles (i.e., Mie theory) predict that c_p and b_{bp} are influenced by particles belongings to different size fractions (Morel

and Ahn, 1991; Stramski and Kiefer, 1991). As a specific example, Mie theory predicts that 50% of b_p is due to particles <3.2 µm, while 50% of b_{bp} is from particles <0.2 µm, if phytoplankton-like particles that follow a power-law (i.e., Junge) size distribution with exponent of –4 are considered (Stramski and Kiefer, 1991). Thus, the relationship between b_{bp} and phytoplankton abundance may not be as strong as for c_p and would depend on the conserved nature of the particle size distribution (PSD) (i.e., that small particles covary with phytoplankton-sized particles).

One of the problems with using Mie theory to simulate backscattering coefficients is that oceanic microorganisms are *not* homogenous spheres. Theoretical models that account for internal structure and non-sphericity of the particles predict backscattering coefficients significantly higher (up to an order of magnitude) than those expected for equivalent homogeneous spheres (Meyer, 1979; Kitchen and Zaneveld, 1992; Quirantes and Bernard, 2004; Clavano et al., 2007). Moreover, direct laboratory measurements of the backscattering coefficient (or the volume scattering function) of phytoplankton cultures are also in disagreement with predictions based on the homogeneous spherical model. For example, Vaillancourt et al. (2004) showed that observed backscattering efficiency factors could be reproduced by Mie theory only by using refractive indices significantly higher than those expected for phytoplankton. Similarly, Volten et al. (1998) concluded that theoretical predictions could not achieve a "good agreement" with their measured volume scattering functions because these predictions are "too steep" in the forward direction (i.e., the backscattering ratio b_{bp}:b_p predicted by Mie theory is too small). Quinby-Hunt et al. (1989) demonstrated that the elements of the scattering matrix measured on a *Chlorella* culture could be satisfyingly reproduced only by a coated-sphere model. When the volume-average of the refractive indices fitted for the coating and for the core of the modeled cell was used as input to the homogeneous spherical model, backscatter was overestimated by a factor 3. Furthermore, Stramski and Piskozub (2003) indirectly determined the backscattering ratios of two species of marine phytoplankton to be between at least three and ten fold larger than those predicted by Mie theory. The above comparisons between theory and

observations were conducted by independent researchers and provide strong evidence that the homogeneous spherical model is insufficient to accurately model the shape of the volume scattering function and the backscattering coefficient of phytoplankton cells.

On the other hand, other investigators have estimated the backscattering of phytoplankton and bacteria by using Mie theory and measuring the volume scattering function over a limited range of backward angles (between about 130 and 170°) (Morel and Ahn, 1990, 1991; Ahn et al., 1992). Results from these studies were in good agreement with the homogeneous spherical model and presented backscattering coefficients for phytoplankton too small to account for the bulk b_{bp} measured in the open ocean. These authors thus concluded that a large fraction of the measured bulk b_{bp} must be due to a group of particles in the submicron size range that has not been well characterized and that seems to be mostly composed of detritus and colloids. Stramski and Kiefer (1991) modeled microorganisms as homogeneous spherical particles and came to similar conclusions. Thus, contrasting results have been presented so far with respect to the backscattering properties of oceanic microorganisms (Stramski et al., 2004).

The current study focuses on the relationship between c_p and b_{bp} in open-ocean surface waters. We find a close correlation between c_p and b_{bp} using high temporal resolution b_{bp} and c_p data collected along a 9000 km-long transect. Backscattering from particles smaller than 0.2 µm was negligible and backscattering from particles in the phytoplankton size range (0.5–20 µm) contributed a significantly greater proportion of the bulk b_{bp} than predicted by Mie theory. These findings and the relatively constant shape of the particle size distribution in open-ocean environments provide supporting evidence to the use of b_{bp} as an alternative to chl-*a* for quantifying phytoplankton abundance from space.

2 Methods

2.1 Flow-through measurements

Flow-through measurements were conducted on the clean seawater supply (intake at 3 m depth) of the R.V. *Ka'imi Moana* during a Tropical Atmosphere Ocean cruise from 8 May to 5 June 2007. The cruise track covered three sides of a rectangle that approximately spanned from 125° W to 140° W and between 10° S and 10° N. During the final leg of the cruise, the ship journeyed over a transect from 10° N 140° W to the Hawaiian islands (Fig. 1). Temperature, salinity and position were recorded by the ship's underway system. To remove bubbles, the seawater supply was plumbed through two vortex debubblers in series (model VDB-1G, diameter of about 5 cm, Stony Brook, NY, USA). Sample water was then distributed to the optical instruments. To account for the dissolved signals, instrumental drifts, and biofouling, a custom-made automatic valve directed the bulk seawater through a 0.2-µm Cole Palmer nylon cartridge filter, for ten minutes every hour. On twelve occasions along the cruise, the sample water arriving from the debubblers was manually diverted through a 3.0-µm Cole Palmer nylon cartridge filter for at least 20 min to measure the contribution from particles smaller than 3 µm to the bulk inherent optical properties.

Beam-attenuation coefficients were measured at 526 and 650 nm by two 25-cm WET Labs C-star transmissometers (sampling rate 5.8 Hz). The wavelengths corresponding to the emission maxima of the light sources, λ_c, of each transmissometer were determined after the cruise by using a spectrally calibrated radiometer (OceanOptics USB2000) and were found to be shifted from the manufacturer declared values by –6 and –10 nm, respectively. Hyperspectral beam attenuation and absorption coefficients were also measured between 400 and 750 nm by a 25-cm WET Labs spectral absorption and attenuation meter (AC-s, sampling rate 3.9 Hz).

The volume scattering function at a central angle of about 117°, $\beta(117°)$ ($m^{-1}\,sr^{-1}$), was measured by a WET Labs ECO-BB3 Measurement Sensor at three wavelengths (470, 526 and 656 nm, sampling rate 1 Hz). The reported λ_c for the backscattering

BGD
6, 291–340, 2009

meter were also determined spectroradiometrically and were found to differ from the stated WET Labs values by 0, –6, and –4 nm, respectively. Instrument gains were increased by the manufacturer before the cruise to measure the low $\beta(117^{\circ})$ values expected in the Equatorial Pacific waters and in the oligotrophic North Pacific Subtropical Gyre. The instrument was operated in a custom-made flow-through chamber that is described in detail in Slade et al. (2009). Briefly, the instrument light sources illuminate the water sample from the bottom of the chamber, thus avoiding accumulation of occasional bubbles on the optical surface. In addition, a baffle in the chamber prevented unwanted photons from reaching the instrument detector. The internal surfaces of the chamber and the baffle were made of black glossy high density polyethylene that minimized diffuse reflectance from the chamber walls (and thus retro-diffusion of unwanted photons into the detector field-of-view). Most of the photons were reflected by the chamber walls in the direction opposite to the instrument, thus favoring their absorption by multiple interactions with the chamber sides and baffle. The chamber volume (about 8.7 l) was conservatively chosen to minimize back-reflections from the chamber sides. A plug (14-cm in diameter) on one of the sides of the chamber was used for installing the instrument and daily cleaning.

Laboratory experiments were carried out to assess the backscattering signal, $b_{b,\mathrm{wall}}$, contributed by reflections off the chamber walls. $b_{b,\mathrm{wall}}$ was determined in replicate experiments by measuring the particulate backscattering of reverse-osmosis water that was recirculated through a 0.2 µm Cole Palmer nylon cartridge filter for about two hours. The resulting $b_{b,\mathrm{wall}}$ values were $(0.25\pm0.10)\times10^{-3}$ and $(0.24\pm0.07)\times10^{-3}\,\mathrm{m}^{-1}$ for the blue and green channels, respectively. We note that such determination might be an overestimate of $b_{b,\mathrm{wall}}$ because the 0.2 µm filtration may leave colloidal particles in the water sample.

$b_{b,\mathrm{wall}}$ should theoretically decrease when natural samples are measured in the flow-through chamber because, as the attenuation by particles or other dissolved substances increases, the photons traveling from the instrument light-source to the chamber wall have a smaller probability of returning to the detector. This decrease in $b_{b,\mathrm{wall}}$

however should be limited since the pathlength covered by these photons is relatively short. We tested this hypothesis by comparing the $b_{b,\text{wall}}$ measured in reverse-osmosis water with that measured when the total absorption coefficient was raised to about 2.0 and 2.2 m^{-1}, in the blue and green channels, respectively, by adding a 0.1 µm-filtered solution of cobalt chlorine. Under these relatively high absorption values, the measured observed decreases in $b_{b,\text{wall}}$ were practically insignificant: $(0.046\pm0.046)\times10^{-3}$ and $(0.030\pm0.030)\times10^{-3}\,\text{m}^{-1}$ in the blue and green channels, respectively. It was therefore decided to consider the values of $b_{b,\text{wall}}$ measured in the laboratory to be constant over the range of optical properties encountered during this study.

Raw digital counts were converted into b_{bp} values by means of the following equation:

$$b_{bp} = 2\pi\chi_p\,[S(C-D) - \beta_{sw}] - b_{b,\text{wall}} \quad (1)$$

where $S(C-D)$ and $[S(C-D)-\beta_{sw}]$ are the total and particle volume scattering functions, β and β_p, respectively; χ_p, taken equal to 1.1, is the factor used to convert the β_p at a central angle of 117° into b_{bp} (Boss and Pegau, 2001); S is the scaling factor determined through a serial dilution with calibrated beads; C are the digital counts; D are the dark counts measured when no light reaches the detector, and β_{sw} is the volume scattering function of pure seawater at the same wavelength and angle at which the BB3 meter measures. To estimate β_{sw}, the model for the volume scattering function of pure water, β_w, proposed by Buiteveld et al. (1994) was used as in Twardowski et al. (2007) with the salinity correction derived from data published by Morel (1974): $\beta_{sw}=\beta_w(1+0.30\text{sal}/37)$, where "sal" is the salinity in practical salinity units. This model for β_{sw} was adopted throughout this study, unless otherwise specified.

The combined experimental uncertainty in b_{bp} was calculated by applying the standard law for the propagation of uncertainty (BIPM and ISO, 1995) to Eq. (1) and assuming uncorrelated uncertainties. The uncertainties of each term of Eq. (1) used in these calculations are reported in Table 1; their median percent squared contributions to the combined b_{bp} uncertainty as well as their median absolute contributions are pre-

BGD
6, 291–340, 2009

sented in Table 2. It is evident that, due to the clarity of the waters under examination, the largest contributor to the uncertainty in b_{bp} was β_{sw}.

During the field study, data from all instruments were time stamped and merged using a WET Labs Data Handler-4. To minimize biofouling effects, all instruments as well as the backscattering flow-chamber were thoroughly cleaned with a mild detergent, diluted ethanol (for glass surfaces only), and deionized water usually every day, and on a few occasions every two days. The 0.2-µm and 3-µm cartridge filters were replaced weekly.

2.2 Particle size distribution measurements

Measurements of particle size distributions (PSDs) were conducted in triplicate with a Coulter Counter Multisizer-3 fitted with a 70-µm aperture tube (which resulted in equivalent spherical diameters, ESD, between 1.4 and 42 µm) at 91 locations along the cruise track. To statistically describe their slopes, a power law was fitted to the differential particle size distribution derived from the Coulter measurements using data points with ESD between 2 and 20 µm and a non-linear routine (Boss et al., 2001).

2.3 Pigment concentrations

Pigment concentrations were measured in several ways. Seawater samples (500 ml) were concentrated on 25-mm Whatman GF/F filters and extracted in 90% acetone for 24 to 36 h in a freezer. The concentration of chlorophyll-*a* (chl-*a*) was determined fluorometrically (Turner Designs) following the acidification method (Strickland and Parsons, 1972). Similarly, size-fractionated chl-*a* was measured after filtering 250 ml of sample on 1-µm and 5-µm Nuclepore polycarbonate filters. Additional 2 l of seawater were filtered on Whatman GF/F filters and stored in liquid nitrogen for high performance liquid chromatography (HPLC) analysis in the laboratory (Hooker et al., 2000; Van Heukelem and Thomas, 2001). Total chlorophyll-*a* concentration, TChl-*a*, was calculated by summing the contributions of monovinyl-chl-*a*, divinyl-

chl-*a* (DivChl-*a*), and chlorophyllide *a*. Chl-*a* was also computed by exploiting the red absorption band of the highly AC-s a_p-spectra (see below). Specifically, chl-*a* was calculated from the particulate absorption line height around 676 nm as chl-a^{ACs}=[a_p(676)−39/65a_p(650)−26/65a_p(715)]/0.014 (e.g., Boss et al., 2007).

An intercalibration of the three different methods for determining chl-*a* was achieved by linearly regressing fluorometric chl-*a* and chl-a^{ACs} against HPLC-derived TChl-*a*. The results of these regressions demonstrated that the intercepts of the above relationships were negligible while the slopes were not significantly different from 1: 1.13 (99% confidence interval: 0.9–2.4) and 1.13 (99% confidence interval: 0.9–1.2), for the fluorometric chl-*a* and chl-a^{ACs}, respectively. The medians of the relative residuals were not significantly different from zero (at the 99% confidence level) and their σ_p were 10.8% and 10.9% for the fluorometric chl-*a* and chl-a^{ACs}, respectively. Thus, chl-a^{ACs} and fluorometric chl-*a* were in agreement with TChl-*a* and no additional correction was applied.

2.4 Flow-through data processing

2.4.1 C-star and AC-s meters

Optical measurements from all instruments were averaged into 1-min time intervals before further processing. To compute particulate beam attenuation and absorption coefficients (c_p and a_p, respectively), the median values of the beam attenuation and absorption coefficients measured during each of the 0.2-µm filtration times were linearly and piecewise interpolated between hours and subtracted from the bulk measurements. This procedure allowed us to determine calibration-independent particulate beam-attenuation and absorption coefficients, with the uncertainties determined mostly by the instrument precision (Boss et al., 2007). AC-s c_p and a_p spectra were further processed to 1) remove a spurious spectral step that was at times observed in the green spectral region (corresponding to the discontinuity in the AC-s filter wheel;

Zaneveld, personal communication), 2) remove the scattering error from the a_p data (method #3, Zaneveld et al., 1994) and 3) account for variations in sample temperature between consecutive 0.2-µm filtered data points (Slade et al., 2009). Finally, the particle scattering coefficient, b_p, was computed as the difference between c_p and a_p.

C-star measurements were processed as for the AC-s to obtain independent c_p values. However, the correction for variation in sample temperature was not applied because the temperature dependence of water absorption around 650 nm can be considered negligible (Sullivan et al., 2006).

2.4.2 Backscattering coefficients

The BB3 meter was calibrated by the manufacturer before the cruise and by the authors after the cruise, to obtain the scaling factors required to convert the digital counts into physical values of $\beta(\lambda_c, 117^\circ)$. Both calibrations were completed using 2-µm beads (Duke Scientific) following established protocols (Moore et al., 2000). The relative difference between the pre- and post-cruise scaling factors was found to be insignificant for the blue and green channels (−4%±5% and −1%±4%, respectively), but a significant positive 15%±2% deviation was found for the red channel that could not be attributed to any specific event during the cruise or the shipment of the meter. In addition, b_{bp} values in the red channel appeared to be contaminated by chl-*a* fluorescence (not shown). Thus, only the blue and green channels of the BB3 were used in the following analysis. The scaling factors were computed as the mean of the pre- and post-cruise measurements. The resulting values and their combined experimental uncertainties (BIPM and ISO, 1995) were: $(6.02\pm0.12)\times10^{-6}$ and $(3.968\pm0.031)\times10^{-6}$ sr^{-1} $count^{-1}$ for the blue and green channels, respectively. Dark readings were determined every two days by covering the detectors with black tape and submerging the instrument in water. The median values (± half the difference between the 84th and 16th percentile, henceforth abbreviated as σ_p) were found to be 53±1 and 56±1 counts for the blue and green channels, respectively. Particle backscattering coefficients were finally calculated from Eq. (1) using the above derived scaling factors and dark counts.

The turnover time of seawater in the flow-through chamber was longer than the 10 min during which the seawater supply was diverted through the 0.2-µm cartridge filter. Thus, the b_{bp} measured during these 10 min never reached a constant minimum value, although it showed the characteristic exponential decay and it decreased by about 75% (Fig. 2a, filled circles). Similarly, measured b_{bp} values exhibited a lag of about 10 min before reaching the bulk b_{bp} signal upon returning the seawater flow to its original, unfiltered path (Fig. 2a, pluses after the filled circles). In addition, the first minute of 0.2-µm filtered data was often noisy. Thus, the first point of the 0.2-µm filtration period, as well as the 10 min of data following the filtration were removed from the analysis (Fig. 2, pluses). The remaining values were used to estimate bulk b_{bp} (Fig. 2a, empty circles). To obtain the "true" backscattering value for the 0.2-µm filtered sample, $b_{bp}(<0.2\,\mu m)$, the b_{bp} values measured during the 0.2-µm filtered measurements, $b_{bp}(t)$, were fitted to the following relation $b_{bp}(t)=b_{bp}(<0.2\mu m)+b_{bp}(t_0)\exp[-s(t-t_0)]$, where t_0 is the first point of the 0.2-µm filtered data used for the fit and s is the decay constant that is proportional to the ratio of the seawater flow rate to chamber volume (Fig. 2, dashed lines). On one occasion, the seawater supply was manually diverted through the 0.2-µm filter for about 50 min and the $b_{bp}(<0.2\,\mu m)$ value extrapolated from the first 9 min of the filtration period was found to be only $10^{-5}\,m^{-1}$ larger than the measured median $b_{bp}(<0.2\,\mu m)$ (Fig. 2b) supporting our extrapolation procedure.

2.4.3 χ_p factor

The $\chi_p(117^\circ)=1.1$ adopted in this study was assumed to be independent of wavelength and obtained from theoretical simulations and experimental field measurements of $\beta_p(\lambda_c, 117^\circ)$ (Boss and Pegau, 2001). However, this $\chi_p(117^\circ)$ value was derived from field and theoretical *continuous* particle size distributions. In the current study, $\beta_p(\lambda_c, 117^\circ)$ was often measured on populations of particles that had been *truncated* by filtration. The applicability of the above χ_p values to truncated particle size distributions was verified by re-examining the theoretical results of Boss and Pegau (2001).

Specifically, the particle-specific volume scattering functions resulting from their simulations were re-weighted using particle size distributions truncated at 0.2, 1, 3, and 5 µm. Figure 3 presents the results of these new integrations and shows that the χ_p values calculated for the truncated particle size distributions do not differ significantly from the value obtained for the continuous particle size distribution around the central angle of the BB3 meter (117°).

While the $\chi_p(117°)$ adopted in this study for continuous particle size distributions is in good agreement with the value (1.08±0.02) obtained by Berthon et al. (2007) from volume scattering functions measured in the North Adriatic Sea, other authors have proposed different values for the χ_p factor. For example, Sullivan et al. (2005) derived a value of 0.90±0.01 at 125° from experimental measurements of the volume scattering function at three angles. On the other hand, Chami et al. (2006) derived a $\chi_p(117°)$ factor of 1.29±0.01 from in-situ measurements in the Black Sea and showed that phytoplankton cultures can display relatively large interspecific differences in χ_p. In addition, the data presented by Chami et al. (2006) suggest that χ_p could be spectrally dependent. Note, however, that the mean value of χ_p^{-1} in the backscattering direction is 1. Given that the VSF of natural populations in the back direction is rather flat, large deviations from 1 are not expected. Finally, the absolute values of b_{bp} obtained from Eq. (1) are directly dependent on the adopted χ_p factors. Thus, caution should be exercised when comparing b_{bp} measurements from different investigators.

2.5 Fractionation experiments

To assess the contribution of different particle sizes to the measured inherent optical properties, three size-fractionation experiments were conducted at three different stations (see locations in Figs. 1 and 4). Measurements of c_p and b_{bp} were conducted on ~20 l of bulk and filtered seawater using AC-s, C-star transmissometers, and BB3 meter in its flow-through chamber. The different size-fractionated samples were obtained by filtering seawater through 0.2-µm Cole Palmer nylon cartridge filters, Whatman GF/F

filters (nominal pore size 0.7 µm, disk diameter 25 mm), 1-µm Nuclepore filters (disk diameter 25 mm), 3-µm Cole Palmer nylon cartridge filters and 5-µm filters (Cole Palmer polypropylene cartridge filters and also Nuclepore, disk diameter 25 mm). For each experiment, instruments were first thoroughly rinsed with filtrate and then optical measurements collected on quiescent samples. A maximum of 1 l of seawater was filtered through each disk-filter to minimize clogging. Finally, the variation of the sample water during the course of the experiment was evaluated by including in the error calculation the changes in bulk IOPs measured at the beginning and at the end of each experiment.

2.6 Mie simulations

2.6.1 Bulk measurements

Mie simulations were completed to assess the ability of Mie theory to reproduce the measured bulk b_{bp} values. The input parameters for these simulations were the PSD, minimum and maximum diameters, and the complex refractive index. Measured PSD were fitted to derive Junge-slopes and the minimum diameter for the simulations was set at 0.2 µm, because the b_{bp}(<0.2 µm) was found to be insignificant (see Results). The imaginary part of the refractive index was assumed to be negligible at the wavelength selected for the simulations (526 nm). To constrain the real part of the refractive index, n, and the maximum value for the diameter, D_{max}, different simulations were executed by simultaneously varying n and D_{max} until agreement was found between modeled and observed c_p and c_p(<3 µm). These two simultaneous constraints were fundamental to obtain a unique set of estimates for n and D_{max}, assuming that the imaginary part was negligible (i.e., particles were assumed not absorbing at 526 nm). The derived n=1.04 and D_{max}=6 µm were then employed to simulate b_{bp}. The core routine for the simulations was based on Bohren and Huffman (1983).

2.6.2 Fractionation experiments

Simulations were also carried out to test the ability of Mie theory to reproduce the c_p and b_{bp} measured during the three fractionation experiments. Particle size distributions (PSDs) of bulk samples were truncated in correspondence of the nominal pore sizes of the filters and used as input for the simulations. Measured PSDs were extrapolated from 1.4 to 0.3 µm using the slope fitted between 2 and 20 µm. The lower limit of the size range used for the fit (2 µm) was selected to avoid a peak observed around 1.5 µm in the PSD measured during the first fractionation experiment (see Results). This peak was fitted using a Gaussian model and added to the Junge distribution adopted for the extrapolation to lower sizes. To reduce uncertainties due to the extrapolation of the PSD to lower sizes, c_p and b_{bp} for the size fractions smaller than 0.7 µm were assumed as known (from our measurements) and only the c_p and b_{bp} generated by size fractions larger than 0.7 µm were modeled. The sensitivity of our results to this hypothesis was investigated by repeating the simulations assuming that the 0.7 µm filter had instead trapped particles >0.3 and >1 µm. n (at 526 nm) and D_{max} were derived as for the bulk measurements described above. However, to further show the sensitivity to the real part of the refractive index (relative to water), simulations were carried out for the following values: 1.02, 1.05, 1.08, and 1.10. The imaginary part of the refractive index was again set equal to zero.

2.7 IOP validation using radiometric data

Hyperspectral remote-sensing reflectance measurements, R_{rs}, were collected at four stations during the cruise by deploying a calibrated Satlantic hyperspectral tethered spectral radiometer buoy (HTSRB). Raw below-surface upward radiance and above-surface downward irradiance data were converted into R_{rs} following Chang et al. (2003). Processing accounted for the depth of the radiance sensor below the sea surface, instrument self-shading errors, and immersion effects.

R_{rs} data at 470 and 526 nm were compared to R_{rs} values modeled as a function

of the coincident IOP data as R_{rs}=$\Re\frac{f}{Q}\frac{b_b}{a}$; were $\Re$=0.53 (Gordon, 2005) accounts for the transfer of radiation across the water-air interface; $\frac{f}{Q}$ describes the bi-directionality of the underwater light field and was derived from the tables presented in Morel et al. (2002); b_b and a are the total backscattering and absorption coefficients, respectively. The measured a_p and the pure water absorption by Pope and Fry (1997) were used to compute a, but the absorption coefficient of chromophoric dissolved organic matter, a_{CDOM}, also needed to compute a, was not available for this cruise. However, a_{CDOM} spectra collected during TAO cruises that covered the same geographic region during 2005 and 2006 were collected following established protocols (Nelson et al., 2004). The median values of $a_{CDOM}(470)$ and $a_{CDOM}(526)$ derived during these cruises in the surface Equatorial Pacific waters were 0.0020 and 0.0007 m^{-1}, respectively, and were included in the computation of a. Modeled remote-sensing reflectances, R_{rs}^{mod}, were found to be in agreement with the observed ones, R_{rs}^{obs}, with biases (median of percent residuals) of –13.1% and –19.2% and random uncertainties (σ_p of percent residuals) of 11.5% and 11.8% in the blue and green channels, respectively (4 observations per channel). Percent residuals were defined as $(R_{rs}^{mod}/R_{rs}^{obs}-1)\times100$.

3 Results

3.1 Bulk measurements

Surface particle beam-attenuation and backscattering coefficients showed a remarkable correlation along the whole cruise track (Fig. 4a), and displayed up to 4-fold variations that were related to both the large latitudinal hydrographic features and to finer scale variability in the water masses sampled (Fig. 4d). b_{bp} and c_p (or b_p) were tightly correlated both at 470 and at 526 nm and the fitted relationships could reproduce the observations with a bias of –4% and 6% and a precision of 11% and 9% in the blue and green channels, respectively (bias and precision are defined as the median and

σ_p of the relative residuals.) Our observations were also found in general agreement with published bio-optical models (Fig. 5).

While both surface chlorophyll-*a* and particle concentrations tracked c_p and b_{bp}, the former displayed larger relative variations (up to 8-fold) than the latter (Fig. 4b). b_{bp}:c_p and b_{bp}:chl-*a* ratios exhibited relatively constant average values with superimposed second order temporal and spatial variability (Fig. 4c).

b_{bp} was positively related to chlorophyll-*a* concentration, and in good agreement with the model proposed by Morel and Maritorena (2001) and Huot et al. (2008) (Fig. 6a and b). On the other hand, existing bio-optical models overestimated the observed b_p values by about 15% (Fig. 6c and d).

The slopes of the Junge-type fits were symmetrically distributed around a median value ($\pm\sigma_p$) of 3.49±0.35. Thus, the shape of particle size distributions was relatively constant in the sampled region for sizes varying between 2 and 20 µm.

3.2 Along track size-fractionated IOPs

Particles smaller than 3 µm contributed 53%±7% and 51%±7% of the bulk b_{bp} measurements at 470 and 526 nm, respectively, and 46%±9% and 40%±5% of the bulk c_p at 526 and 650 nm, respectively (Fig. 7a, b.) The fraction of chl-*a* originating from particles smaller than 1 µm was generally higher than the ratio DivChl-*a*:TChl-*a* (Fig. 7c) and accounted for 51%±15% of the total chl-*a*. Panel (d) of Fig. 7 shows that, when concurrent data were available (unfortunately, only on two occasions), the fraction of chl-*a* originating from particles <3 µm and derived from filtered AC-s measurements was between the chl-*a* originating from particles <1 and <5 µm.

3.3 Mie simulations for bulk measurements

Figure 8a and b shows the simulated and observed c_p and fractional c_p(<3 µm) obtained using the optimized n=1.04 and D_{max}=6 µm as input for the simulations. Two other values of the refractive index are also presented. Figure 8c and d presents the

simulated backscattering coefficient and its fractional contribution by particles <3 µm obtained from the same optimized n and D_{max}. The homogeneous spherical model constrained with the above parameters was unable to accurately reproduce the observed b_{bp}. The median ($\pm\sigma_p$) ratio of simulated to observed b_{bp} was 0.11±0.05. Thus, the simulations accounted for about 10% of the measured b_{bp} and suggested that most of b_{bp} was due particles smaller than 3 µm (Fig. 8d).

3.4 Fractionation experiments

The first fractionation experiment took place at the equator (0°, 140° W) in relatively mesotrophic conditions (TChl-a=0.25 mgm^{-3}, bulk c_p(526)=0.14 m^{-1}; Figs. 1 and 4c). The differential particle distribution measured on bulk samples showed a peak centered around 1.5 µm superimposed on a Junge-like shape and presented the largest total number of particles of the three experiments. The second and third experiments were completed in the more oligotrophic north Pacific gyre (9° N, 140° W, and 15.4° N, 150.4° W, respectively; TChl-a=0.07 and 0.04 mgm^{-3}, bulk c_p(526)=0.054 and 0.039 m^{-1}, respectively; Figs. 1 and 4c) and presented smoother particle size distributions and significantly lower numbers of particles between 1.4 and 40 µm (12 529, 5202, and 2920 particles per ml for the 1st, 2nd, and 3rd experiments, respectively).

During the first fractionation experiment, approximately 68% and 80% of the bulk b_{bp} and c_p signals, respectively, were generated by particles greater than 0.7 µm (Fig. 9a, b). Approximately 58% of the bulk b_{bp} was generated by particles greater than 3 µm. In the more oligotrophic waters sampled during the 2nd and 3rd experiments, particles greater than 0.7 µm contributed 71% and 43% of the bulk b_{bp} respectively (Fig. 9c–f). This size fraction however, contributed about the same percentage of the bulk c_p signal, i.e. 83% and 85%, respectively (Fig. 9c–f).

Simulation results indicated that, in general, Mie theory required higher refractive indices to match the b_{bp} than the c_p measurements although uncertainties in measured b_{bp} are rather large in the third fractionation experiment (Fig. 9). This mismatch may

be due to an underestimation of the predicted efficiency factor for backscattering. Alternative explanations could be that b_{bp} and c_p were sensitive to two different particle populations (e.g., Brown and Gordon, 1974; Zaneveld et al., 1974), or that the two optical properties recorded changes in different morphological characteristics of the same particle population (e.g., the overall cell vs. the cell wall, Meyer, 1979). The sensitivity analysis showed that variability in the filtration efficiency of the 0.7 µm filters used as baselines for the simulations did not introduce uncertainties large enough to explain the mismatch in refractive index between b_{bp} and c_p.

3.4.1 Mie simulations with observed size-fractionated PSDs for the 3rd fractionation experiment

The Mie simulations carried out for the three fractionation experiments were based on PSDs of bulk samples that were set to zero above the diameters corresponding to the nominal pore sizes of the filtered samples. This approach was taken because PSD measurements were not collected on the size-fractionated samples during the 1st and 2nd experiments. However, a limited set of PSDs were measured on the size-fractionated samples collected during the 3rd fractionation experiment.

Figure 10 presents the PSDs measured on the size-fractionated samples collected during the 3rd experiment. As expected, PSD measurements of the 0.7-µm filtered sample were practically indistinguishable from the blanks (0.2-µm filtered seawater) over the range of sizes presented in the figure. Similarly, the PSDs of the 5-µm filtered sample matched the bulk sample PSDs for ESD smaller than 5 µm (above that ESD, the data were too noisy).

However, the 1-µm and the 3-µm filtered samples presented some problems. The PSD of the 1-µm filtered sample had, as expected, values similar to those measured on the bulk sample at bin sizes of about 1.4 µm, but showed that some particles with ESD up to 1.5 µm had passed through the filter (Fig. 10, compare red lines with black stars). This phenomenon may be explained by imperfect filter pores (e.g., two pores in contact with each other), by large soft particles that disaggregated as they passed

through the filter and re-aggregated afterwards, and/or by an incorrect nominal pore size of the filter. On the other hand, the PSD of the 3-µm filtered sample retained a significant fraction of particles smaller than the nominal pore size.

Mie simulations were repeated using the PSDs measured on the size-fractionated samples and extrapolated to 0.3 µm. The PSD measured for the size fraction smaller <1 µm was much steeper than the observed bulk PSD. Thus, to avoid biasing the simulation, this PSD was extrapolated to 0.7 µm by employing the slope of the bulk PSD.

Results for the 1- and 5-µm size fractions were consistent with those obtained using the truncated bulk PSDs (compare thick black lines with large circles in Fig. 9e, f). However, the new b_{bp} and c_p values simulated for the 3-µm size fraction were lower than those obtained from the truncated bulk PSD.

In conclusion, the PSD data measured on the size-fractionated samples during the 3rd fractionation experiment were in general agreement with the measured size-fractionated IOPs, exception made for the PSD collected for 3-µm size fraction.

3.5 Backscattering from 0.2-µm filtered samples

Figure 11a shows that the hourly b_{bp}(<0.2 µm) data were remarkably constant along the cruise track and accounted for an insignificant fraction of the bulk signal even though the b_{bp}(<0.2 µm) values for the blue channel were systematically larger than the green ones. The ratio of the extrapolated b_{bp}(<0.2 µm) to the last point of the 0.2-µm filtered b_{bp} had a median value ($\pm\sigma_p$) of 0.85±0.09, suggesting that the 0.2-µm filtration time was generally long enough to flush out most of the particles from the chamber. The times when b_{bp}(<0.2 µm) showed local maxima (9 May and 1 June) corresponded to local maxima in the bulk b_{bp} values (compare with Fig. 4c). In those occasions the 10-min 0.2-µm filtration time may not have been long enough and, as a consequence, the b_{bp}(<0.2 µm) extrapolated from the fits were inaccurate. Another explanation could be that there might have been residual bubbles in the sample water. Finally, the coefficients of determination for the linear relationships between b_{bp}(<0.2 µm) and other variables such as chl-*a*, bulk b_{bp}, c_p, temperature and salinity

were always smaller than 0.07.

Twardowski et al. (2007) in a recent review found that the most commonly used models of β_w (Morel, 1974; Shifrin, 1988; Buiteveld et al., 1994) predict values of β_w within ±6%, if the same value for the depolarization ratio is adopted. However, these authors have also pointed out that further research is needed to corroborate the predictions of the salinity correction: the correction applied to β_w to account for the increased scattering due to dissolved salts. To investigate this effect, the above calculations were repeated using the β_w model proposed by Buiteveld et al. (1994) with the salinity correction proposed by Shifrin (1988): a linear increase in scattering by water up to 39% at a salinity of 35 psu and a temperature of 20°C (Shifrin, 1988, his Table 3.13, page 96). The resulting b_{bp}(<0.2 µm) displayed reduced spectral dependencies, and were considerably closer to zero than those obtained with Morel's (1974) salinity correction (Fig. 11b).

4 Discussion

4.1 Bulk inherent optical properties

In this study continuous measurements of bulk inherent optical properties and discrete biogeochemical parameters have been presented for surface waters of the Equatorial Pacific during May 2007. In addition to the bulk measurements, size-fractionated data on b_{bp}, c_p, a_p, and chl-*a* were collected and analyzed. Other investigators have studied size-fractionated c_p and a_p in the oligotrophic Crater Lake (Boss et al., 2007), size-fractionated b_{bp} measurements in productive coastal waters (Roesler and Boss, 2008), and size-fractionated c_p in the Equatorial Pacific (Chung et al., 1996). Here, for the first time to the best of our knowledge, size-fractionated b_{bp} data are presented for open-ocean waters and a comparison of different size-fractionated inherent optical properties is undertaken.

Two technical and methodological innovations were critical for the collection of the

data set presented in this study. First, highly accurate calibration-independent flow-through measurements of particulate beam-attenuation and absorption coefficients were achieved by applying a correction based on temporally adjacent 0.2-µm filtered measurements (Slade et al., 2009). Second, a novel custom-made flow-through chamber allowed continuous surface particle backscattering measurements.

The accuracy of the measured inherent optical properties was determined through favorable comparison between measured R_{rs} values and R_{rs} modeled using the measured IOPs (see Method section), as well as through closure of c_p with Mie theory (Figs. 8a and b and 9b, d and f). In addition, median b_{bp}:b_p ratios ($\pm\sigma_p$) were consistent with the ranges reported for other oligotrophic waters (i.e., 0.0103±0.0013 and 0.0094±0.0011, at 470 and 526 nm, respectively; Whitmire et al., 2007; Stramski et al., 2008, but see Twardowski et al., 2007).

Particle backscattering and beam-attenuation (or scattering) coefficients were tightly correlated (Fig. 5) and in agreement with other studies and published bio-optical models (Loisel and Morel, 1998; Morel and Maritorena, 2001; Huot et al., 2008). Despite the absence from our data of previously observed diel cycles in c_p (e.g., Siegel et al., 1989), both the b_{bp}:c_p and b_{bp}:chl-*a* ratios showed such cycles (compare Fig. 4a and c). It may be argued that these cycles arise because b_{bp} and c_p are sensitive to different particle populations (e.g., small vs. large) whose temporal dynamics are out of phase. However, an alternative explanation may be that these variations resulted from differences in the sensitivities of b_{bp} and c_p to morphological changes in the same average particle population, or that they arise because of biases in c_p due to the finite acceptance angle of the transmissometer (Boss et al., unpublished). Finally, variations in b_{bp}:c_p were limited and did not compromise the overall covariation between b_{bp} and c_p.

Taken together our findings imply that a common particle pool contributes, at least in part, to both b_{bp} and c_p. In agreement with this conclusion, Junge-slopes derived by fitting Coulter counter data between 2 and 20 µm varied by about 10% along the cruise and a significant fraction of b_{bp} originated from particles in the phytoplankton

size range (see below).

4.2 Size-fractionated inherent optical properties

The along-track 3-µm filtrations, as well as the fractionation experiments, demonstrated that particles smaller than 3 µm directly contributed about 40% and 50% of the bulk particulate and backscattering coefficients, respectively, in the mesotrophic regions sampled (Figs. 7a and 9a). Fractional c_p data for particles <3 µm were found in agreement with the range of fractional c_p for particles <8 µm (41–89%) reported by Chung et al. (1996).

The size fraction <3 µm contributed less to c_p (Figs. 7b and 9b, f) than to b_{bp}, in qualitative agreement with the prediction that the total scattering coefficient is sensitive to particles larger than those influencing b_{bp} (Morel and Ahn, 1991; Stramski and Kiefer, 1991). However, the absolute contributions by this size fraction were different from those expected from Mie theory. Stramski and Kiefer (1991) analyzed the sensitivity of their simulations to the slope of the assumed Junge-like PSD and found that 50% of b_{bp} originated from particles <1.2 µm, while 50% of b_p was due to particles <5.7 µm, for an index of refraction of 1.05 (typical of "soft" organic particles) and a PSD slope of –3.5 (similar to the one measured in this study). Thus, in our measurements, more backscattering (and less scattering) originated from large particles than predicted by Mie theory.

4.3 b_{bp}(<0.2 µm)

Another important observation recorded during this study was the relatively constant and statistically insignificant backscattering of 0.2 µm-filtered seawater, b_{bp}(<0.2 µm) (Fig. 11). There were no evident changes in b_{bp}(<0.2 µm) when the 0.2 µm cartridge filters were replaced during the cruise (black arrows in Fig. 11). Thus, filter clogging and retention of particles <0.2 µm did not appear significant. This finding, if verified, is important because it contradicts previous theoretical predictions that attributed about

50% of b_{bp} to particles smaller than 0.2 µm (when the Junge-slope is –4, Fig. 4b in Stramski and Kiefer, 1991).

4.4 Size-fractionation by filtration

The fractionated backscattering and beam-attenuation coefficients reported in this study were determined by filtration of seawater samples. Filtration is a technique widely used in oceanographic research to partition the continuous size distribution that naturally occurs in water samples. For example, Ciotti et al. (2002) used data on size-fractionated chlorophyll concentration to parameterize a size-dependent model of phytoplankton absorption. Other investigators have used size-fractionation to relate the bloom of specific phytoplankton groups to nanomolar increases in nitrate in the Sargasso Sea (Glover et al., 1988) or to follow the seasonal cycle of phytoplankton blooms (Clarke and Leakey, 1996).

Despite its widespread use, size-fractionation based on filtration has its disadvantages. Filters can retain a significant fraction of particles smaller than the declared pore size and the amount of this unwanted fraction depends on the particle stickiness coefficient and on the filter type (Sheldon, 1972; Logan, 1993; Logan et al., 1994; Chavez et al., 1995; Knefelkamp et al., 2007). The main reason for the mismatch between nominal pore sizes and actual retained sizes appears to be filter clogging and the inability to accurately define the pore size of filters (e.g., Droppo, 2000). Filter clogging was minimized during our 0.2- and 3-µm filtrations by means of cartridge filters with large surface areas (0.64 m^2) and by replacing filters frequently. In addition, the filtration of samples in-situ should have minimized particle aggregation and precipitation. Clogging and statistical fluctuations of our results were further decreased during our large-volume size-fractionation experiments by filtering small amounts of sample through each filter.

The following considerations are presented as evidence that the results obtained from the fractionation experiments were minimally affected by filter clogging and, thus provide a reasonable representation of size-fractionated IOPs. First, the validity of the

fractionated-chl-*a* measurements is established by noting that a significantly smaller fraction of chl-*a* was retained by the 1 μm- than by the 0.7 μm-filters (range 0.2–0.7, median 0.5) (Fig. 7d), indicating that the 1.0 µm filters did not retain considerable amounts of particles smaller than their pore size. Moreover, the <1 µm size fraction typically retained more chl-*a* than the DivChl-*a*:TChl-*a* values derived from the HPLC analysis (Fig. 7c). Since DivChl-*a* is a pigment typical of the genus *Prochlorococcus* with typical average diameter of 0.5–0.7 µm (e.g. Grob et al., 2007), this observation independently verifies that the 1-µm Nuclepore filters were not trapping a significant number of particles smaller than their pore size. Similarly, samples processed through disk filters during the fractionation experiments should not have been significantly affected by filter clogging, to the extent that the larger seawater volumes filtered during the fractionation experiments did not cause significant obstruction of filter pores. This hypothesis was partially validated by the only two fractional chl-*a* values derived from the along-cruise 3-µm filtered a_p measurements and concurrent to the size-fractionated chl-*a* (Fig. 7d). Finally, effective partitioning of the size distribution is also evidenced by the closure (in terms of refractive index range) achieved between Mie simulations and measurements of the fractionated c_p (Figs. 8b and 9b, d, f). Thus, although not perfect, measurements of size-fractionated water samples can provide important insights on the relative contributions of different particles to the bulk inherent optical properties. Future investigations should stress collection of comprehensive ancillary measurements, including particle size distributions, for each size fraction.

4.5 Comparison of observations with Mie theory

Open-ocean waters are dominated by organic particles with typical refractive indices of 1.02 to 1.05 (e.g., Zaneveld and Pak, 1973; Carder et al., 1972). By applying these values we found predictions by Mie theory to be in agreement with c_p measurements (Figs. 8a, 9b, d, f). In contrast, simulated b_{bp} was underestimated by almost an order of magnitude when the refractive index that matched the c_p data was used as input for the b_{bp} simulations. Similarly, significant contributions to b_{bp} from size fractions >0.7 µm

could only be accounted for in Mie calculations by using refractive indices higher than 1.05 (Fig. 9a, c, e). These results indicate that either b_{bp} and c_p were sensitive to two different populations of particles whose abundances were tightly correlated (Fig. 5), or that our data are in agreement with many previous independent theoretical and experimental studies that document the inability of the homogeneous spherical model to reproduce phytoplankton backscattering coefficients and the relative shape of their volume scattering functions (Meyer, 1979; Zielinski et al., 1986, 1987; Quinby-Hunt et al., 1989; Kitchen and Zaneveld, 1992; Volten et al., 1998; Vaillancourt et al., 2004; Quirantes and Bernard, 2006).

A likely reason for the above deficiency is the sensitivity of the shape of the volume scattering function (but not of total scattering) to the internal structure and non-sphericity of natural particles (Meyer, 1979; Kitchen and Zaneveld, 1992; Quirantes and Bernard, 2004; Clavano et al., 2007). In other words, the relative amount of light scattered in the backward direction is higher for a microorganism that contains internal organelles and membranes than for a homogeneous sphere with the same average refractive index. Unfortunately, the large diversity of plankton and theoretical limitations of b_{bp} modeling of non-spherical particles (e.g., Clavano et al., 2007) has so far limited the parameterization and use of models more complex than the homogeneous sphere for predicting optical properties of the open ocean.

Importantly, other authors have determined considerably smaller backscattering coefficients of microorganisms than those found in the aforementioned studies (Morel and Ahn, 1990, 1991; Ahn et al., 1992). It is noteworthy, however, that these experiments were all based on the same technique and hypotheses: conversion of the measured volume scattering function at a narrow angular range into b_{bp} using Mie theory. Thus, contrasting results are obtained depending on the measurement technique and the assumptions made. More investigations are required to clarify this important issue.

4.6 χ_p of coated spheres

One aspect of our analysis that may appear a contradiction to our overall conclusions is that the χ_p factor at 117° adopted in this study was predicted by Mie theory and found to be in agreement with experimentally determined χ_p values (e.g., Boss and Pegau, 2001; Berthon et al., 2007). Recognition of this detail might incorrectly suggest that Mie theory is indeed able to accurately predict the b_{bp} of natural particles. However, this contradiction is resolved by considering that the use of the homogeneous or the coated cell models causes large differences in the simulated b_{bp}:b_p ratio, but has only a minor impact on the b_{bp}:$\beta_p(117^\circ)$ ratio (i.e., χ_p). To test this hypothesis we conducted a preliminary investigation where a coated spherical model (based on algorithms by Bohren and Huffman, 1983) was used to simulate the volume scattering functions of particles distributed between 0.4 and 100 µm according to a Junge-type power law with exponents between –3 and –4. Particle sizes were determined by the radius of the core plus the thickness of the shell. We assumed that the shell thickness can either have a constant value of 75 nm (Meyer, 1979), or be a constant (i.e., 5%) fraction of the core radius (Kitchen and Zaneveld, 1992). The refractive index of the core was varied between 1.015 and 1.025, while that of the shell between 1.085 and 1.095 (Kitchen and Zaneveld, 1992). Thus, the volume-averaged refractive indices had median values of 1.05 (range: 1.047–1.057) and 1.03 (range: 1.025–1.035), for the first and second type of coated models, respectively. Particles were considered non-absorbing. This analysis revealed that the resulting χ_p values around 117° were consistent with the values obtained from the homogeneous spherical model (Fig. 3). On the other hand, the median backscattering ratio derived from the coated-sphere model with shell thickness of 75 nm was 0.011 (range: 0.0063–0.0180), while that for the coated-sphere model with shell thickness equal to 5% of the core radius was 0.0085 (range: 0.0064–0.0180). Thus, the backscattering ratios were about a factor 2.2 and 1.7, respectively, larger than those derived from the homogeneous spherical model (median: 0.005, range: 0.0035–0.0074) using the same size distributions and

BGD
6, 291–340, 2009

refractive index equal to 1.05. In conclusion, it appears that the χ_p value adopted in this study is consistent with non-homogeneous models of phytoplankton cells that produce relatively large b_{bp}:b_p ratios. It should be noted, though, that different combinations of shell thickness and refractive indices may produce significantly different backscattering ratios (both higher and lower). A thorough investigation of the optimal coated shell model for phytoplankton, however, is beyond the scope of this work.

4.7 Final remarks

A direct influence of particles in the phytoplankton size range on b_{bp} and the conserved shape of the particle size distribution create a close correspondence between b_{bp} and c_p variability (Fig. 5). These findings add to previous studies that have 1) suggested that c_p can track phytoplankton abundances (Durand and Olson, 1996; Chung et al., 1996, 1998; Green et al., 2003; Oubelkheir et al., 2005); 2) shown that chl-*a*:c_p ratios are closely correlated to variations in phytoplankton physiological parameters in the field (Behrenfeld and Boss, 2003); and 3) demonstrated that the ratio of chl-*a* to a function of b_{bp} retrieved from ocean color data tracks physiological trends expected from laboratory experiments over vast oceanic regions (Behrenfeld et al., 2005). Together, these different lines of evidence add support to the hypothesis that b_{bp} can provide an alternative to chl-*a* for monitoring open-ocean phytoplankton biomass from space (Behrenfeld et al., 2005; Westberry et al., 2008). It is additionally noteworthy that chlorophyll-*a* concentrations during our Equatorial Pacific study spanned a range (0.05 to 0.4 $\mathrm{mg\,m^{-3}}$) representative of about 80% of the open ocean (based on satellite chl-*a* retrievals). Accordingly, our results are likely relevant to many open-ocean regions, as has already been established for the South Pacific (Huot et al., 2008). Further verification is nevertheless desirable.

5 Conclusions

A field data set of bulk and size-fractionated measurements of inherent optical properties was presented and analyzed for the surface waters of the Equatorial Pacific during May 2007. These are the key findings and implications:

- b_{bp} and c_p were highly correlated, suggesting that either particle scattering property should be equally valued as a remote-sensing proxy for phytoplankton biomass in open-ocean waters.
- The slope of the particle size distribution between 2 and 20 µm was found to be rather constant (3.49±0.35) along the whole cruise.
- b_{bp} measurements of 0.2-µm filtered seawater were relatively constant across the sampled region and did not contribute a significant fraction of the bulk b_{bp}.
- Particles larger than 3 µm contributed in median 50% of b_{bp}.
- Predictions based on the homogeneous spherical model could only account for about 10% of the measured b_{bp}.

Acknowledgements. The authors would like to thank the captain and crew of the R. V. Ka'imi Moana for making this study possible. WET Labs is kindly acknowledged for providing the technical drawings used for designing the flow-through backscattering chamber and for assistance in operating the BB3 meter. C. Roesler kindly provided the HTSRB used for in this study. R. O'Malley is acknowledged for providing the MODIS AQUA chl-*a* estimates. NASA funding is acknowledged under contracts NNG05GD18G, NNG05GD16G, and NNG05GR50G to M.J.B.

References

Ahn, Y., Bricaud, A., and Morel, A.: Light backscattering efficiency and related properties of some phytoplankters, Deep-Sea Res., 38, 1835–1855, 1992. 296, 317

Behrenfeld, M. J. and Boss, E.: The beam attenuation to chlorophyll ratio: an optical index of phytoplankton physiology in the surface ocean?, Deep-Sea Res. Pt. I, 50, 1537–1549, 2003. 294, 319

Behrenfeld, M. J., Boss, E., Siegel, D. A., and Shea, D. M.: Carbon-based ocean productivity and phytoplankton physiology from space, Global Biogeochem. Cy., 19, 1–14, doi:10.1029/2004GB002299, 2005. 294, 319

Berthon, J. F., Shybanov, E., Lee, M. E. G., and Zibordi, G.: Measurements and modeling of the volume scattering function in the coastal northern Adriatic Sea, Appl. Optics, 46, 5189–5203, 2007. 304, 318

BIPM and ISO: Guide to the Expression of Uncertainty in Measurement, International Organization for Standardization, Geneve, Switzerland, 1995. 299, 302

Bohren, C. F. and Huffman, D. R.: Absorption and Scattering of Light by Small Particles, Wiley, New York, 1983. 305, 318

Boss, E. and Pegau, W. S.: Relationship of light scattering at an angle in the backward direction to the backscattering coefficient, Appl. Optics, 40, 5503–5507, 2001. 299, 303, 318, 331

Boss, E., Twardowski, M. S., and Herring, S.: Shape of the particulate beam attenuation spectrum and its inversion to obtain the shape of the particulate size distribution, Appl. Optics, 40, 4885–4893, 2001. 300

Boss, E. S., Collier, R., Larson, G., Fennel, K., and Pegau, W. S.: Measurements of spectral optical properties and their relation to biogeochemical variables and processes in Crater Lake, Crater Lake National Park, OR, Hydrobiologia, 574, 149–159, 2007. 301, 312

Brown, O. B. and Gordon, H. R.: Size-refractive index distribution of clear coastal water particulates from light scattering, Appl. Optics, 13, 2874, 1974. 310

Buiteveld, H., Hakvoort, J. H. M., and Donze, M.: The Optical Properties of Pure Water, SPIE Vol. 2258, pp. 174–183, 1994. 299, 312

Carder, K. L., Tomlinso, R. D., and Beardsle, G. F.: Technique for estimation of indexes of refraction of marine phytoplankters, Limnol. Oceanogr., 17, 833–839, 1972. 316

Chami, M., Marken, E., Stamnes, J. J., Khomenko, G., and Korotaev, G.: Variability of the relationship between the particulate backscattering coefficient and the volume scattering function measured at fixed angles, J. Geophys. Res.-Oceans, 111, 1–10, doi:10.1029/2005JC003230, 2006. 304

Chang, G. C., Dickey, T. D., Mobley, C. D., Boss, E., and Pegau, W. S.: Toward closure of upwelling radiance in coastal waters, Appl. Optics, 42, 1574–1582, 2003. 306

Chavez, F. P., Buck, K. R., Bidigare, R. R., Karl, D. M., Hebel, D., Latasa, M., Campbell, L., and Newton, J.: On the chlorophyll-a retention properties of glass-fiber GF/F filters, Limnol. Oceanogr., 40, 428–433, 1995. 315

Chung, S. P., Gardner, W. D., Richardson, M. J., Walsh, I. D., and Landry, M. R.: Beam attenuation and micro-organisms: Spatial and temporal variations in small particles along 140 degrees W during the 1992 JGOFS EqPac transects, Deep-Sea Res. Pt. II, 43, 1205–1226, 1996. 293, 312, 314, 319

Chung, S. P., Gardner, W. D., Landry, M. R., Richardson, M. J., and Walsh, I. D.: Beam attenuation by microorganisms and detrital particles in the equatorial Pacific, J. Geophys. Res.-Oceans, 103, 12 669–12 681, 1998. 293, 319

Ciotti, A. M., Lewis, M. R., and Cullen, J. J.: Assessment of the relationships between dominant cell size in natural phytoplankton communities and the spectral shape of the absorption coefficient, Limnol. Oceanogr., 47, 404–417, 2002. 292, 315

Clarke, A. and Leakey, R. J. G.: The seasonal cycle of phytoplankton, macronutrients, and the microbial community in a nearshore Antarctic marine ecosystem, Limnol. Oceanogr., 41, 1281–1294, 1996. 315

Claustre, H., Morel, A., Babin, M., Cailliau, C., Marie, D., Marty, J. C., Tailliez, D., and Vaulot, D.: Variability in particle attenuation and chlorophyll fluorescence in the tropical Pacific: Scales, patterns, and biogeochemical implications, J. Geophys. Res.-Oceans, 104, 3401–3422, 1999. 292, 293

Clavano, W. R., Boss, E., and Karp-Boss, L.: Inherent optical properties of non-spherical marine-like particles from theory to observation, Oceanogr. Mar. Biol. Annu. Rev., 45, 1–38, 2007. 295, 317

Cole, J. J., Findlay, S., and Pace, M. L.: Bacterial production In fresh and saltwater ecosystems – A cross-system overview, Mar. Ecol.-Prog. Ser., 43, 1–10, 1988. 293

Droppo, I. G.: Encyclopedia of analytical chemistry, chap. Filtration in Particle Size Analysis, John Wiley & Sons Ltd, Chichester, pp. 5397–5413, 2000. 315

Durand, M. D. and Olson, R. J.: Contributions of phytoplankton light scattering and cell concentration changes to diel variations in beam attenuation in the equatorial Pacific from flow cytometric measurements of pico-, ultra- and nanoplankton, Deep-Sea Res. Pt. II, 43, 891–906, 1996. 293, 319

Gasol, J. M. and Duarte, C. M.: Comparative analyses in aquatic microbial ecology: how far do they go?, Fems Microbiol. Ecol., 31, 99–106, 2000. 293

Geider, R. J., MacIntyre, H. L., and Kana, T. M.: A dynamic regulatory model of phytoplanktonic acclimation to light, nutrients, and temperature, Limnol. Oceanogr., 43, 679–694, 1998. 294
Glover, H., Prezelin, B., Campbell, L., Wyman, M., and Garside, C.: A nitrate-dependent Synechococcus bloom in surface Sargasso Sea water, Nature, 331, 161–163, 1988. 315
Gordon, H. R.: Normalized water-leaving radiance: revisiting the influence of surface roughness, Appl. Optics, 44, 241–248, 2005. 307
Gordon, H. R. and Morel, A.: Remote Assessment of Ocean Color for Interpretation of Satellite Visible Imagery. A Review. Springer-Verlag, New York, 1983. 335
Green, R. E., Sosik, H. M., and Olson, R. J.: Contributions of phytoplankton and other particles to inherent optical properties in New England continental shelf waters, Limnol. Oceanogr., 48, 2377–2391, 2003. 293, 319
Grob, C., Ulloa, O., Claustre, H., Huot, Y., Alarcon, G., and Marie, D.: Contribution of picoplankton to the total particulate organic carbon concentration in the eastern South Pacific, Biogeosciences, 4, 836–852, 2007, http://www.biogeosciences.net/4/836/2007/. 293, 316
Hooker, S. B., Claustre, H., Ras, J., Van Heukelem, L., Berthon, J.-F., Targa, C., van der Linde, D., Barlow, R., and Session, H.: The first SeaWiFS HPLC analysis round-robin experiment (SeaHARRE-1), NASA Technical Memorandum – SeaWIFS Postlaunch Technical Report Series no.14, pp. 40–42, 2000. 300
Huot, Y., Morel, A., Twardowski, M. S., Stramski, D., and Reynolds, R. A.: Particle optical backscattering along a chlorophyll gradient in the upper layer of the eastern South Pacific Ocean, Biogeosciences, 5, 495–507, 2008, http://www.biogeosciences.net/5/495/2008/. 294, 308, 313, 319, 334, 335
Kitchen, J. C. and Zaneveld, J. R. V.: A three-layered sphere model of the optical properties of phytoplankton, Limnol. Oceanogr., 37, 1680–1690, 1992. 295, 317, 318
Knefelkamp, B., Carstens, K., and Wiltshire, K. H.: Comparison of different filter types on chlorophyll-a retention and nutrient measurements, J. Exp. Mar. Biol. Ecol., 345, 61–70, 2007. 315
Logan, B. E.: Theoretical analysis of size distributions determined with screens and filters, Limnol. Oceanogr., 38, 372–381, 1993. 315
Logan, B. E., Passow, U., and Alldredge, A. L.: Variable retention of diatoms on screens during size separations, Limnol. Oceanogr., 39, 390–395, 1994. 315
Loisel, H. and Morel, A.: Light Scattering and Chlorophyll Concentration in Case 1 Waters: a

Reexamination, Limnol. Oceanogr., 43, 847–858, 1998. 294, 313, 334, 335
Meyer, R. A.: Light-scattering from biological cells – Dependence of backscatter radiation on membrane thickness and refractive-index, Appl. Optics, 18, 585–588, 1979. 295, 310, 317, 318
Moore, C., Twardowski, M., and Zaneveld, J.: The ECO VSF: A multi-angle scattering sensor for determination of the volume scattering function in the backward direction, in: Ocean Optics XV, SPIE, Office of Naval Research, pp. 16–20, 2000. 302
Morel, A.: Optical properties of pure water and pure seawater, in: Optical Aspects of Oceanography, edited by: Jerlov, N. G. and Nielsen, S. E., Academic Press, pp. 1–24, 1974. 299, 312
Morel, A. and Ahn, Y. H.: Optical-efficiency factors of free-living marine-bacteria – influence of bacterioplankton upon the optical-properties and particulate organic-carbon in oceanic waters, J. Mar. Res., 48, 145–175, 1990. 296, 317
Morel, A. and Ahn, Y. H.: Optics of heterotrophic nanoflagellates and ciliates – a tentative assessment of their scattering role in oceanic waters compared to those of bacterial and algal cells, J. Mar. Res., 49, 177–202, 1991. 294, 296, 314, 317
Morel, A. and Maritorena, S.: Bio-pptical properties of oceanic waters: a reappraisal, J. Geophys. Res.-Oceans, 106, 7163–7180, 2001. 308, 313, 334, 335
Morel, A., Antoine, D., and Gentili, B.: Bidirectional reflectance of oceanic waters: accounting for raman emission and varying particle scattering phase function, Appl. Optics, 41, 6289–6306, 2002. 307
Nelson, N. B., Carlson, C. A., and Steinberg, D. K.: Production of chromophoric dissolved organic matter by Sargasso Sea microbes, Mar. Chem., 89, 273–287, 2004. 307
Oubelkheir, K. J., Claustre, H., Sciandra, A., and Babin, M.: Bio-optical and biogeochemical properties of different trophic regimes in oceanic waters, Limnol. Oceanogr., 50, 1795–1809, 2005. 293, 319
Pope, R. M. and Fry, E. S.: Absorption spectrum (380–700 nm) of pure water. 2. Integrating cavity measurements, Appl. Optics, 36, 8710–8723, 1997. 307
Quinby-Hunt, M. S., Hunt, A. J., Lofftus, K., and Shapiro, D.: Polarized-light scattering studies of Marine Chlorella, Limnol. Oceanogr., 34, 1587–1600, 1989. 295, 317
Quirantes, A. and Bernard, S.: Light scattering by marine algae: two-layer spherical and non-spherical models, J. Quant. Spectrosc. Ra., 89, 311–321, 2004. 295, 317
Quirantes, A. and Bernard, S.: Light-scattering methods for modelling algal particles as a col-

lection of coated and/or nonspherical scatterers, J. Quant. Spectrosc. Ra., 100, 315–324, 2006. 317
Roesler, C. and Boss, E.: Real-time coastal observing systems for marine ecosystem dynamics and harmful algal blooms: theory, instrumentation and modelling, chap. In situ measurement of the inherent optical properties and potential for harmful algal bloom detection and coastal ecosystem observations, UNESCO, pp. 153–206, 2008. 312
Sheldon, R. W.: Size separation of marine seston by membrane and glass-fiber filters, Limnol. Oceanogr., 17, 494–498, 1972. 315
Shifrin, K. S.: Physical Optics of Ocean Water, Springer-Verlag, 1988. 312
Siegel, D., Dickey, T., Washburn, L., Hamilton, M. K., and Mitchell, B. G.: Optical determination of particulate abundance and production variations in the oligotrophic ocean, Deep-Sea Res., 36, 211–222, 1989. 292, 313
Slade, W. H., Dall'Olmo, G., Boss, E., Langner, M. R., Behrenfeld, M. J., and Roesler, C.: A flow-through method for high accuracy along-cruise-track measurement of inherent optical properties, in preparation, 2009.
Stramski, D. and Kiefer, D.: Light scattering by microorganisms in the open ocean, Prog. Oceanogr., 28, 343–383, 1991. 295, 296, 314, 315
Stramski, D. and Piskozub, J.: Estimation of scattering error in spectrophotometric measurements of light absorption by aquatic particles from three-dimensional radiative transfer simulations, Appl. Optics, 42, 3634–3646, 2003. 295
Stramski, D., Boss, E., Bogucki, D., and Voss, K. J.: The role of seawater constituents in light backscattering in the ocean, Prog. Oceanogr., 61, 27–56, 2004. 296
Stramski, D., Reynolds, R. A., Babin, M., Kaczmarek, S., Lewis, M. R., Rottgers, R., Sciandra, A., Stramska, M., Twardowski, M. S., Franz, B. A., and Claustre, H.: Relationships between the surface concentration of particulate organic carbon and optical properties in the eastern South Pacific and eastern Atlantic Oceans, Biogeosciences, 5, 171–201, 2008, http://www.biogeosciences.net/5/171/2008/. 313
Strickland, J. and Parsons, T.: A Practical Handbook of Seawater Analysis, Fisheries Research Board of Canada, 1972. 300
Sullivan, J. M., Twardowski, M. S., Donaghay, P. L., and Freeman, S. A.: Use of optical scattering to discriminate particle types in coastal waters, Appl. Optics, 44, 1667–1680, 2005. 304
Sullivan, J. M., Twardowski, M. S., Zaneveld, J. R. V., Moore, C. M., Barnard, A. H., Don-

aghay, P. L., and Rhoades, B.: Hyperspectral temperature and salt dependencies of absorption by water and heavy water in the 400–750 nm spectral range, Appl. Optics, 45, 5294–5309, 2006. 302

Twardowski, M. S., Claustre, H., Freeman, S. A., Stramski, D., and Huot, Y.: Optical backscattering properties of the "clearest" natural waters, Biogeosciences, 4, 1041–1058, 2007, http://www.biogeosciences.net/4/1041/2007/. 299, 312, 313

Vaillancourt, R. D., Brown, C. W., Guillard, R. R. L., and Balch, W. M.: Light backscattering properties of marine phytoplankton: relationships to cell size, chemical composition and taxonomy, J. Plankton Res., 26, 191–212, 2004. 295, 317

Van Heukelem, L. and Thomas, C. S.: Computer-assisted high-performance liquid chromatography method development with applications to the isolation and analysis of phytoplankton pigments, J. Chromatogr. A, 910, 31–49, 2001. 300

Volten, H., de Haan, J. F., Hovenier, J. W., Schreurs, R., Vassen, W., Dekker, A. G., Hoogenboom, H. J., Charlton, F., and Wouts, R.: Laboratory measurements of angular distributions of light scattered by phytoplankton and silt, Limnol. Oceanogr., 43, 1180–1197, 1998. 295, 317

Westberry, T., Behrenfeld, M., Siegel, D., and Boss, E.: Carbon-based primary productivity modeling with vertically resolved photophysiology, Global Biogeochem. Cy., 22, GB2024, doi:10.1029/2007GB003078, 2008. 319

Whitmire, A. L., Boss, E., Cowles, T. J., and Pegau, W. S.: Spectral variability of the particulate backscattering ratio, Opt. Express, 15, 7019–7031, 2007. 313

Zaneveld, J. and Pak, H.: Method for determination of index of refraction of particles suspended in ocean – Reply, J. Opt. Soc. Am., 63, 321–324, 1973. 316

Zaneveld, J., Roach, D., and Pak, H.: The determination of the index of refraction distribution of oceanic particulates, J. Geophys. Res., 79, 4091–4095, 1974. 310

Zaneveld, J. R. V., Kitchen, J. C., and Moore, C. C.: Scattering error correction of reflecting tube absorption meters, in: Ocean Optics XII, edited by Ackelson, S., vol. 2258, SPIE, pp. 44–55, 1994. 302

Zielinski, K., Król, T., Gedziorowska, D., and Wolinski, L.: Theoretical and experimental investigations into light scattering by the Chlorella vulgaris cell, B. Pol. Acad. Sci.-Earth, 34, 313–319, 1986. 317

Zielinski, K., Król, T., and Gedziorowska, D.: The influence of the inner structure of the Chlorella vulgaris cell on light scattering properties, B. Pol. Acad. Sci.-Earth, 35, 119–125, 1987. 317

Table 1. Experimental uncertainties of each term of Eq. (1) used to compute the combined experimental uncertainty of b_{bp} as a function of wavelength. Units of absolute uncertainties are the same as those reported in the text for the corresponding variables.

Variable	Uncertainty		Reference
	470 nm	526 nm	
χ_p	4.4%	4.4%	Boss and Pegau (2001)
S	1.2×10^{-7}	0.31×10^{-7}	measured
C	1.5	2	measured
D	1	1	measured
β_{sw}	7.8%	7.8%	estimated from Twardowski et al. (2007)
b_{bp}^{w}	5.9×10^{-5}	4.8×10^{-5}	measured

Table 2. Uncertainty budget for b_{bp} based on the values presented in Table 1 and on all BB3 measurements collected during the cruise. Numbers represent the median values of the squared percent contributions, σ^2_{rel} (unitless), and the median absolute contributions, σ (m^{-1}), by each input variable to the combined experimental uncertainty in b_{bp} as a function of wavelength.

Variable	σ^2_{rel}		$\sigma \times 10^{-4}$	
	470 nm	526 nm	470 nm	526 nm
χ_p	5	8	0.42	0.35
S	12	2	0.62	0.17
C	12	21	0.62	0.55
D	5	5	0.42	0.27
β_{sw}	57	49	1.36	0.84
$b_{b,\text{wall}}$	11	16	0.59	0.48

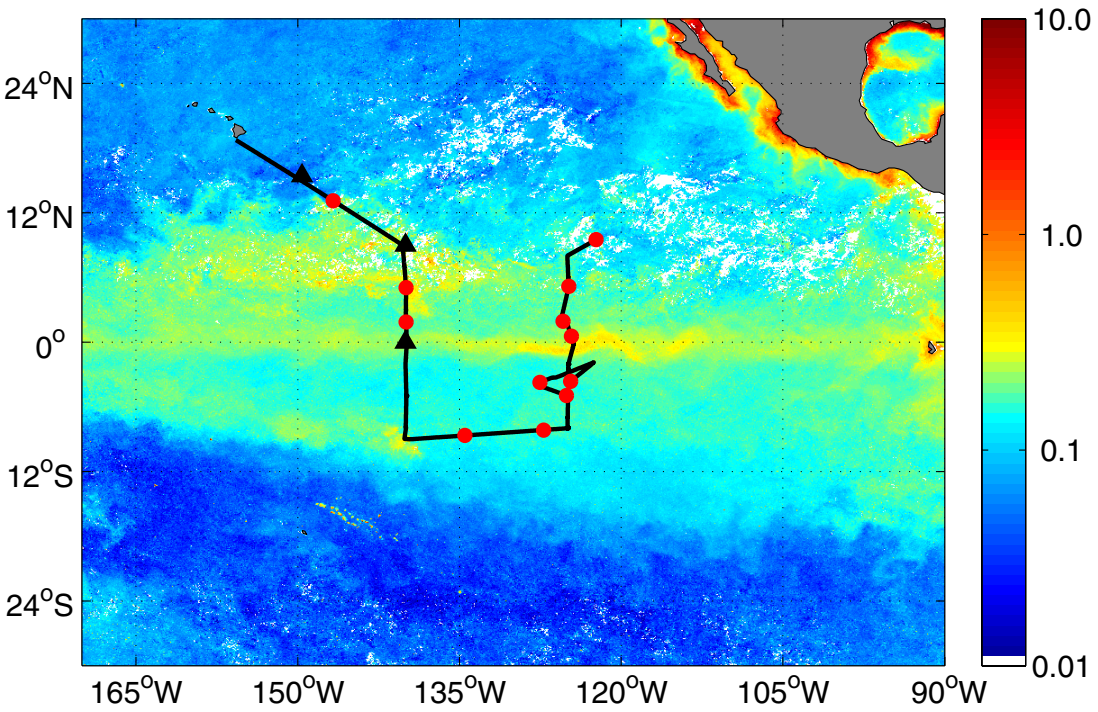

Fig. 1. SeaWiFS chlorophyll-*a* map (units of mg m^{-3}) for May 2007 showing the cruise track (black line) and the locations of the 3-µm filtrations (red circles) and of the fractionation experiments (black triangles). Clouds and land are represented in white and gray, respectively.

BGD
6, 291–340, 2009

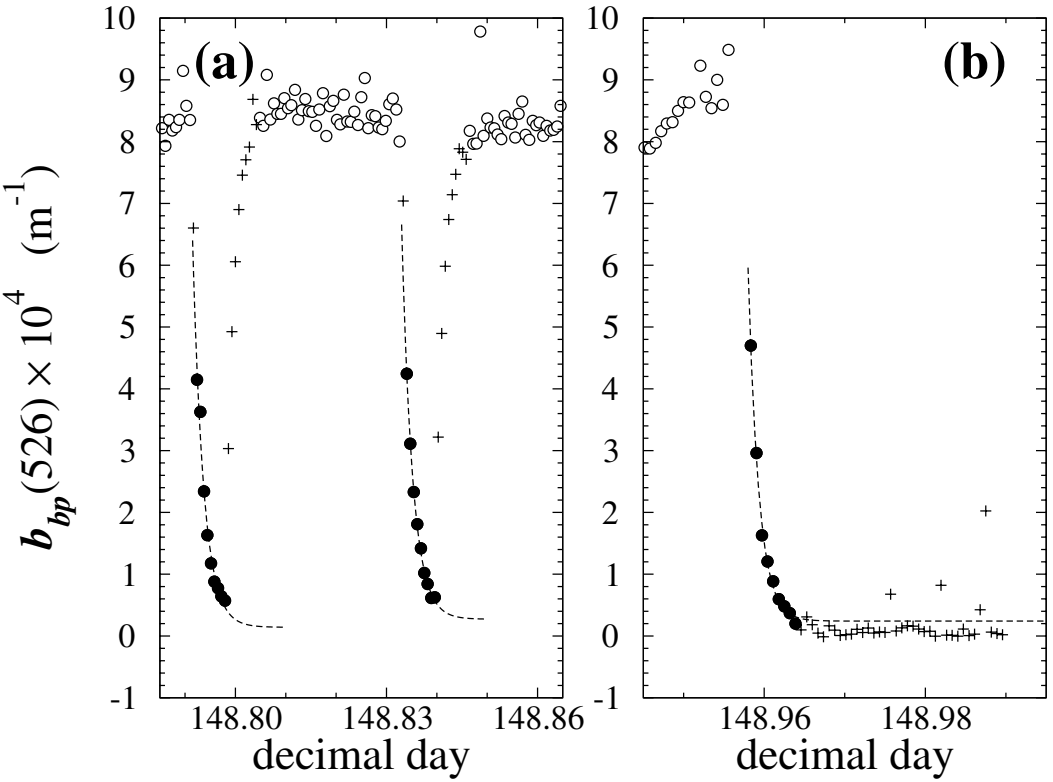

Fig. 2. (a) Example showing bulk b_{bp} measurements used for the analysis (open circles) as well as data collected during the 0.2-µm filtration period (filled circles) that were fitted (dashed line) to derive the 0.2-µm filtered b_{bp}(<0.2 µm) value (obtained as the asymptotic value approached by the dashed line). Pluses indicate data that were excluded from the analysis. **(b)** b_{bp} data from the 50-min 0.2-µm filtration experiment comparing the asymptotic value extrapolated from the fit to the measured b_{bp}(<0.2 µm).

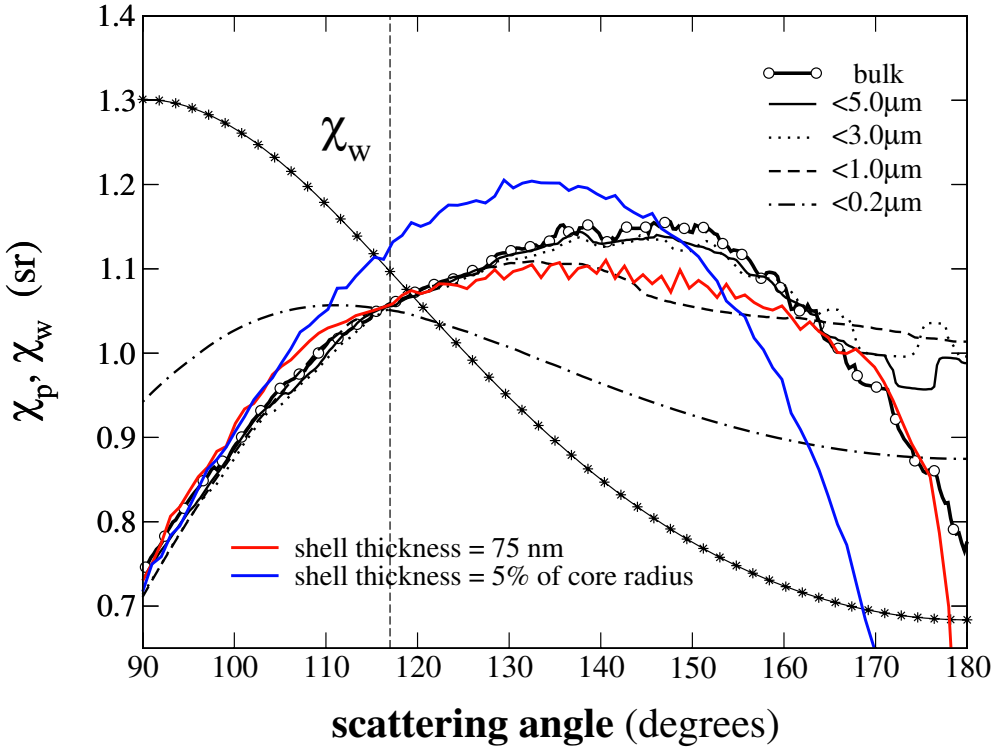

Fig. 3. Median χ_p values computed by re-integrating the theoretical results of Boss and Pegau (2001) using particle size distributions truncated at 0.2, 1, 3, and 5 μm. The median χ_p value for the continuous particle size distributions (indicated as "bulk" in the legend) as well as that for pure water (χ_w) are also reported for reference. The red and blue lines represent the median χ_p values computed for populations of coated, spherical particles with constant shell thickness of 75 nm and shell thickness equal to 5% of the core radius, respectively. The vertical dashed line marks the central angle of the BB3 meter (117°).

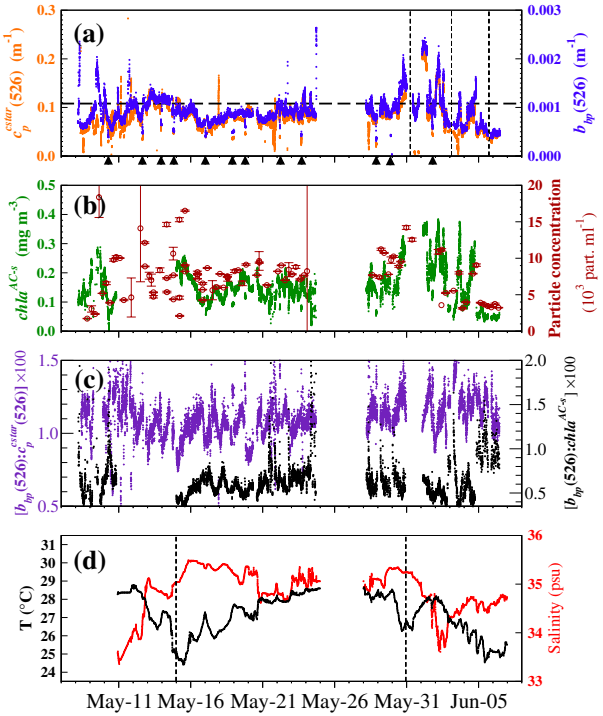

Fig. 4. Time series of data collected along the cruise track. The black triangles and the vertical dashed lines in **(a)** indicate the locations of the 3-µm filtrations and of the fractionation experiments, respectively. The horizontal dashed line in (a) indicates the backscattering of pure sea water at 526 nm which was computed using the model by Buiteveld et al. (1994) and Morel's (1974) salinity correction. The dashed vertical lines in **(d)** mark the beginning and the end of the two equatorial stations. To remove high frequency noise, all optical data plotted in this figure were filtered as follows: first a median filter (window size of 30 min) was applied to each time series and the relative difference ε between the value of the median filter and the actual data computed; then all points for which $\varepsilon \geq 15\%$ were excluded from the plot.

BGD
6, 291–340, 2009

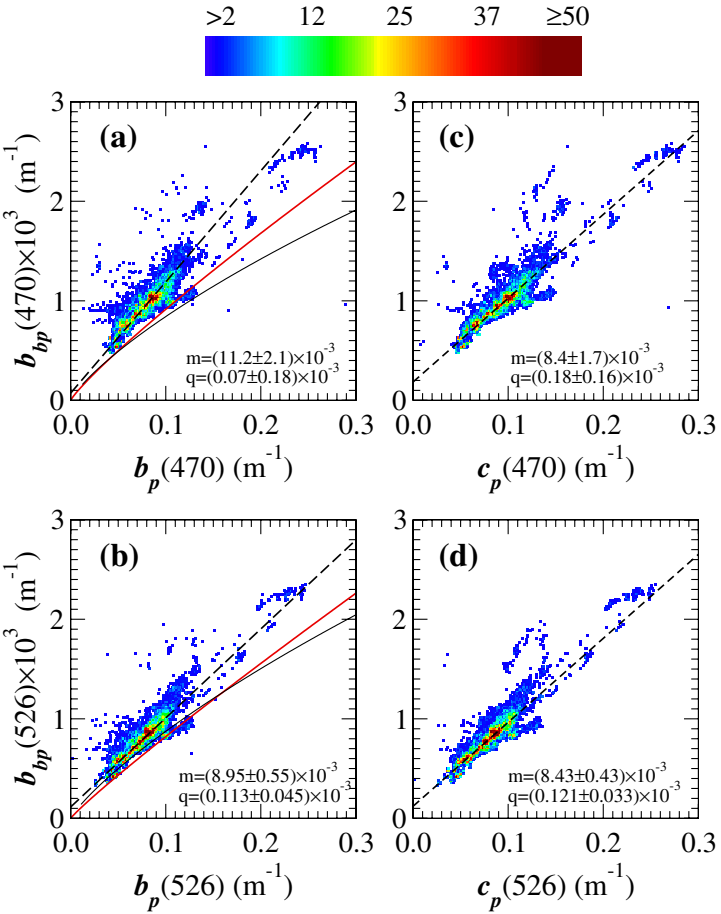

Fig. 5.

BGD
6, 291–340, 2009

Particulate backscattering in the ocean

G. Dall'Olmo et al.

Fig. 5. Bivariate histograms representing the relationships between b_{bp} and c_p (from the AC-s) at the central wavelengths of the BB3 meter. The color bar defines the number of data points per bin, N_{bin}. Continuous red lines represent the relationships obtained, after some algebraic manipulation, from the models derived by Huot et al. (2008) from data collected in the South Pacific. Continuous black lines are derived from the models by Morel and Maritorena (2001) and Loisel and Morel (1998). Note we used for both b_{bp} and b_p the scattering model by Loisel and Morel (1998) that did not include North Atlantic waters (i.e., subsets 2+3 of the homogeneous layer). Binned b_{bp} and c_p were fitted using a weighted linear regression to the function $b_{bp}=m\times c_p+q$ to minimize the leverage of outliers (dashed lines). An iterative technique was used to select the weights which were always integer powers of N_{bin}: the coefficients of the regression were first determined as the median of 100 bootstrapped samples using as weight N_{bin}^n, with n=0. Then n was increased by one and the coefficients and their errors recalculated. The iteration was terminated when the changes in both coefficients were smaller than their uncertainties. Reported uncertainties represent the 99% confidence intervals.

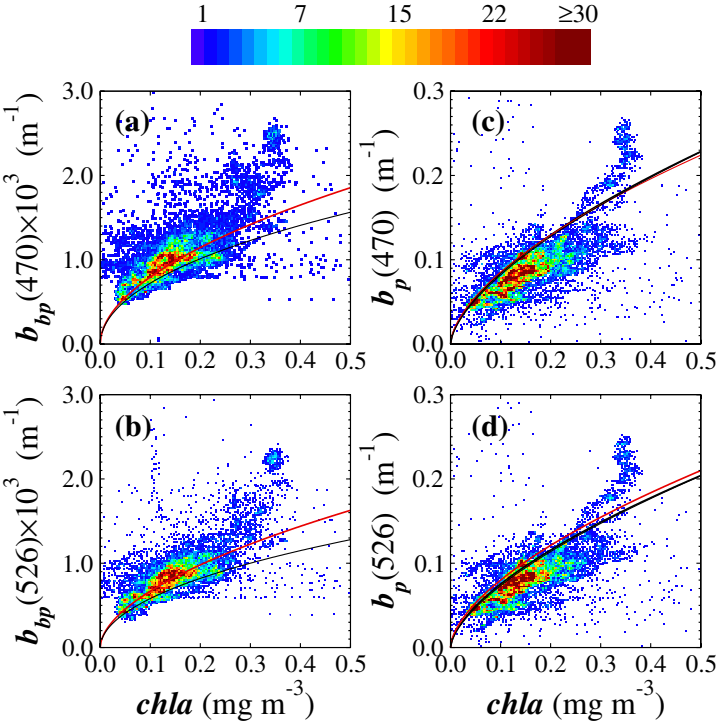

Fig. 6. Bivariate histograms representing the relationships between b_{bp} and chl-*a* (obtained from the AC-s) and b_p and chl-*a* at 470 and 526 nm. Black lines in **(a)** and **(b)** are predictions from the model by Morel and Maritorena (2001). Continuous and dashed black lines in **(c)** and **(d)** are predictions from the models by Gordon and Morel (1983) and Loisel and Morel (1998), respectively, scaled to the corresponding wavelengths assuming a λ^{-1} spectral dependency. Red lines represent the models derived by Huot et al. (2008). The scattering model by Loisel and Morel (1998) that did not include data from the North Atlantic (i.e., subsets 2+3 of the homogeneous layer) was used.

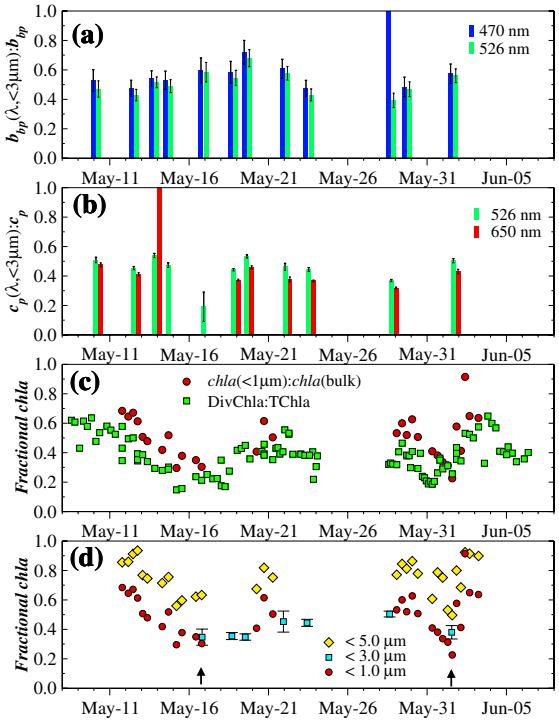

Fig. 7. Fractions of b_{bp} and c_p smaller than 3 µm, **(a)** and **(b)**, respectively; error bars represent combined experimental uncertainties. **(c)** relationship between the fraction of chl-*a* due to particles smaller than 1 µm obtained from the size-fractionated chl-*a* measurements, and the HPLC-derived fractional contribution of divinyl chl-*a* to TChl-*a*. **(d)** fractional contributions to chl-*a* from particles <1 and <5 µm (derived form the fractionated chl-*a* measurements) and from particles <3 µm (derived from filtered a_p measurements). Black arrows in (d) indicate the two concurrent AC-s and fractionated chl-*a* measurements.

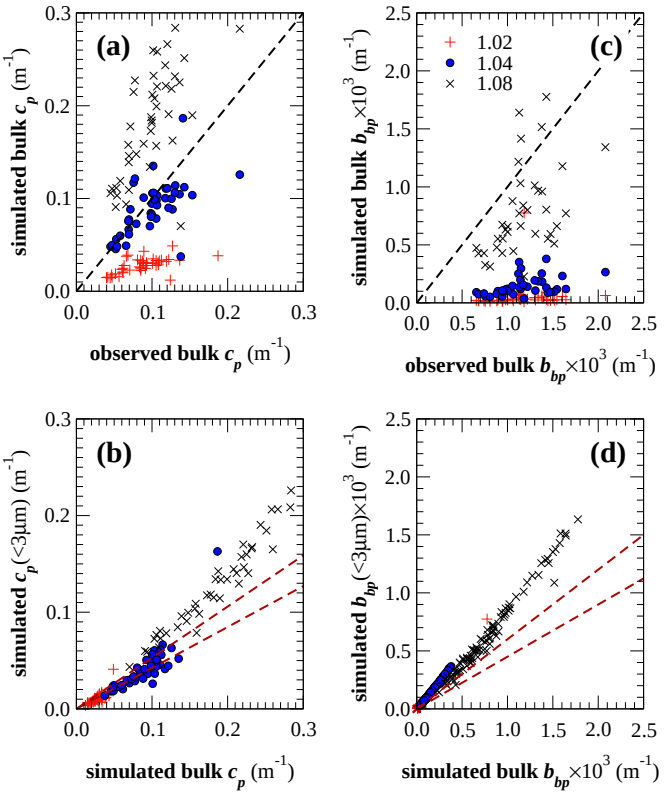

Fig. 8. Simulated vs. observed bulk c_p and b_{bp} at 526 nm **(a)** and **(c)**, respectively. Simulated bulk c_p and b_{bp} vs. simulated c_p(<3 μm) and b_{bp}(<3 μm) at 526 nm **(b)** and **(d)**, respectively. 1:1 lines are marked in **(a)** and **(c)**. Brown dashed lines in **(b)** and **(d)** represent the observed ranges of fractional c_p(<3 μm) and b_{bp}(<3 μm). Different symbols refer to different refractive indices as indicated in the legend.

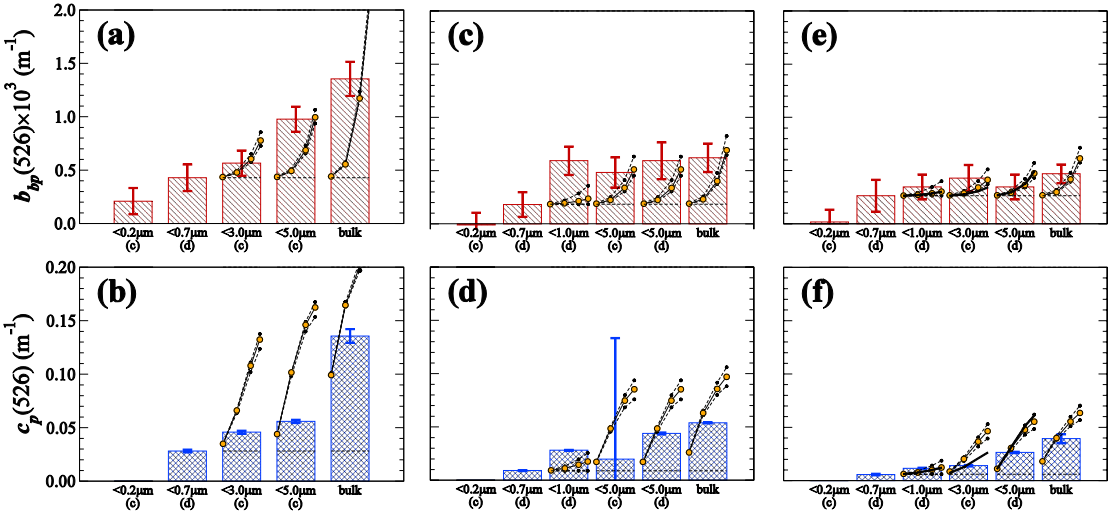

Fig. 9. Particle backscattering (top) and beam-attenuation (bottom) coefficients at 526 nm for the first **(a, b)**, second **(c, d)**, and third **(e, f)** fractionation experiments. Bars represent measured IOPs for the indicated size fractions, the rightmost bars represent the bulk measurements. Error bars represent combined experimental uncertainties. Lines with symbols are results from Mie simulations for the size fractions larger than 0.7 µm and smaller than the sizes reported below each bar (see text for details). Horizontal dashed lines mark the b_{bp} **(a)** and c_p **(b)** values recorded for the size fraction <0.7 µm. Modeled b_{bp} and c_p values for different refractive indices are presented (from left to right: 1.025, 1.05, 1.075, and 1.10). The letters in parentheses below the bars indicate the type of filter used: c=cartridge, d=disk. Optimal values derived from fitting c_p were: n=1.05 and D_{max}=16 µm (a, b), n=1.05 and D_{max}=9 µm (c, d), and n=1.05 and D_{max}=12 µm (e, f). Thick continuous lines in (e, f) represent simulations completed using the PSDs measured on each size-fractionated sample.

BGD
6, 291–340, 2009

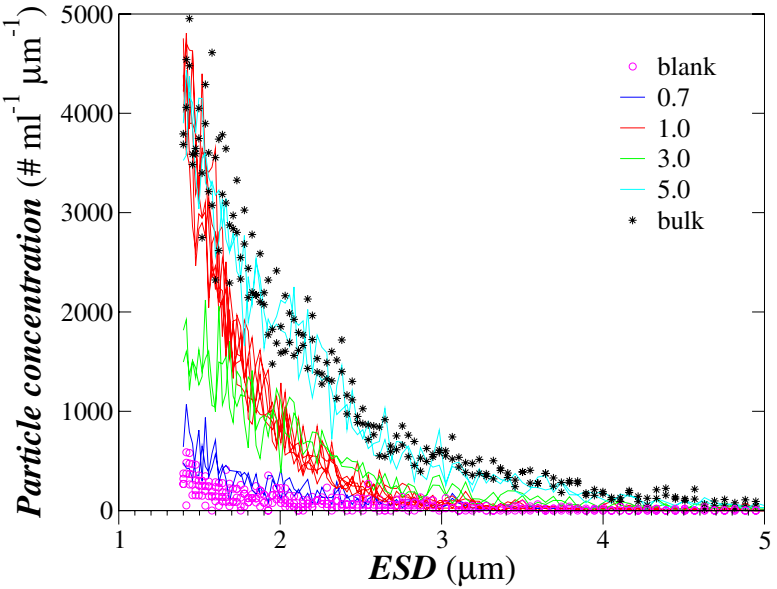

Fig. 10. Particle size distribution measurements for the size-fractionated samples collected during the 3rd fractionation experiment. Lines of a given color represent multiple measurements on the same size-fractionated sample and thus, provide an estimate of the instrumental precision.

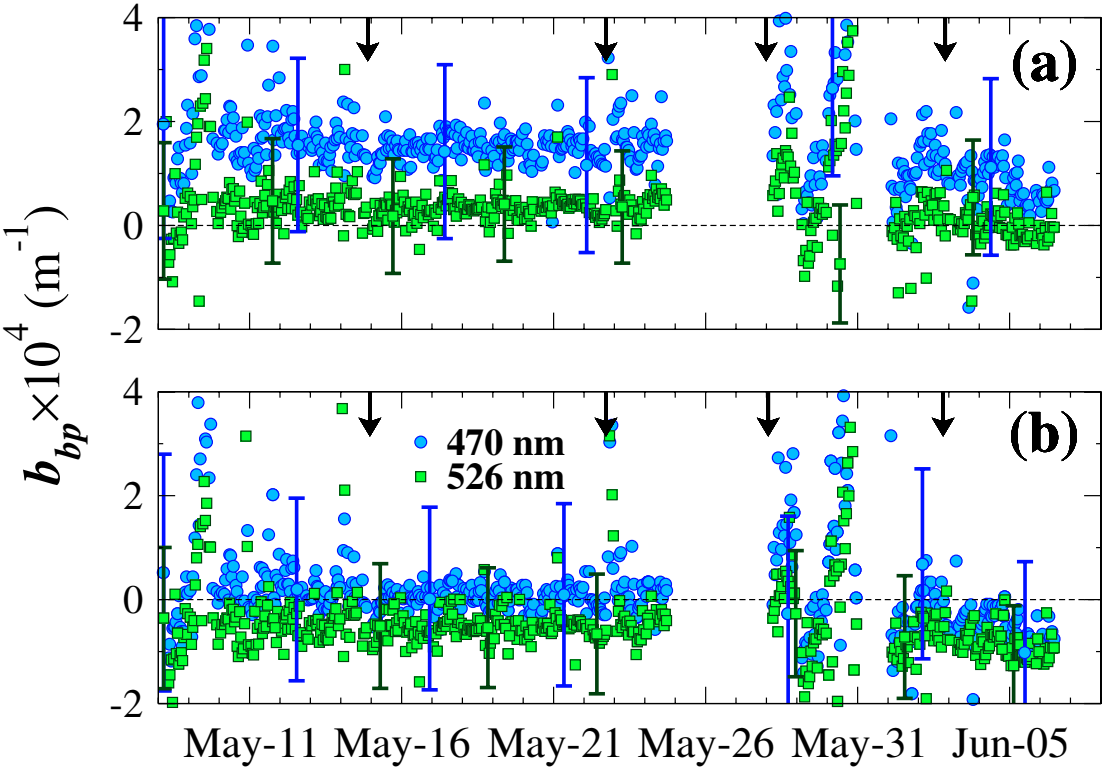

Fig. 11. b_{bp}(<0.2 µm) data as a function of wavelength extrapolated from the hourly 0.2-µm filtered b_{bp} measurements (see text for details). Arrows indicate the times when the 0.2-µm cartridge filters were changed. Data obtained using the β_w modeled according to Buiteveld et al. (1994) with **(a)** Morel's (1974) salinity correction and **(b)** with the salinity correction proposed by Shifrin (1988).

BGD
6, 291–340, 2009